livers

MDPI

Article

Defining Gene Signature of Tumor-Associated Macrophages in Intrahepatic Cholangiocarcinoma as Target for Immunotherapy Using Single Cell and Bulk RNA Sequencing

Joshua S. Badshah [1], Ryan M. Lee [1], Andrea Reitsma [1], Marc L. Melcher [1], Olivia M. Martinez [1], Sheri M. Krams [1], Daniel J. Delitto [2] and Varvara A. Kirchner [1,*]

[1] Division of Abdominal Transplantation, Department of Surgery, Stanford University, Stanford, CA 94305, USA; rmlee2354@gmail.com (R.M.L.); melcherm@stanford.edu (M.L.M.)
[2] Division of Complex Surgical Oncology, Department of Surgery, Stanford University, Stanford, CA 94305, USA
* Correspondence: kirc0079@stanford.edu

Abstract

Background: Intrahepatic cholangiocarcinoma (ICC) has a poor prognosis due to late-stage presentation and ineffective systemic therapies. Targeting the tumor microenvironment (TME) in ICC offers new therapeutic possibilities, particularly through tumor-associated macrophages (TAM), which can both promote and inhibit tumor progression. The current study utilized multi-omics analysis to characterize the gene signature of TAM and explore its therapeutic potential in ICC. **Methods:** Public GEO datasets provided the basis for analysis. Single-cell RNA sequencing (scRNA-seq) data from five ICCs, three adjacent non-tumorous tissues (ANTs), and four healthy liver samples were examined with Python. To validate scRNA-seq findings, bulk RNA-seq data from 27 ICC and 27 matched ANT samples were assessed using R. Differentially expressed genes were identified with adjusted *p*-values <0.01 and log2-fold changes >1 or <−1. CIBERSORT pipeline analyzed 22 immune cell subtypes in bulk RNA-seq data. STRING database analyzed the contribution of unique TAM-related genes to networks of protein–protein interactions. **Results:** TAM population demonstrated phenotypic heterogeneity exhibiting partial gene signatures of inflammatory (MS1) and anti-inflammatory (MS2) macrophages. Unique TAM-associated markers, TREM2, CD9, and PRMT10, showed variable expression within the TAM subpopulation. Bulk RNAseq analysis confirmed the scRNA-seq results, highlighting overexpression of TREM2 and CD9 in most ICC samples versus ANT. Immune cell deconvolution revealed decreased MS1 and MS2 macrophages in ICC, and alterations in adaptive immune profile, suggesting immunotolerant TME. STRING database defined TREM2-LGALS3 axis as a potential target for anti-tumor therapies. **Conclusions:** TAM represents a unique heterogenous population which is primarily found in ICC TME versus ANT or healthy liver tissue The non-uniform expression of unique gene signature demonstrates additional heterogeneity in the TAM subpopulation and suggests that TREM2+ TAM may be desirable targets for anti-TREM2-LGALS3 immunotherapy.

Keywords: intrahepatic cholangiocarcinoma; tumor-associated macrophages; single cell RNS sequencing; TREM2

Academic Editors: Ralf Weiskirchen and Veronika Lukacs-Kornek

Received: 26 August 2025
Revised: 1 October 2025
Accepted: 23 October 2025
Published: 29 October 2025

Citation: Badshah, J.S.; Lee, R.M.; Reitsma, A.; Melcher, M.L.; Martinez, O.M.; Krams, S.M.; Delitto, D.J.; Kirchner, V.A. Defining Gene Signature of Tumor-Associated Macrophages in Intrahepatic Cholangiocarcinoma as Target for Immunotherapy Using Single Cell and Bulk RNA Sequencing. *Livers* **2025**, *5*, 53. https://doi.org/10.3390/livers5040053

1. Introduction

Intrahepatic cholangiocarcinoma (ICC) is the second most common type of primary liver cancer [1]. Historically, the incidence of ICC has had the highest prevalence in Asian countries [2]; however, over the past four decades, the incidence rates have been increasing in the Western hemisphere [3,4]. Complete resection of ICC is the only curative option with overall survival (OS) of 50% at 3 years. Unfortunately, more than 80% of cases progress beyond surgical resection due to the extent of the tumor at the time of the diagnosis, leaving systemic therapy as the only option with 3-year OS at 5% [1]. The poor efficacy of current systemic therapies exposes a need for new modalities such as immunotherapies, where modulation of cellular immune response can be effective against ICC [5].

Tumor-associated macrophages (TAM), a subtype of myeloid immune cells that are recruited and activated in the tumor microenvironment (TME), present an attractive new target for prognostic and therapeutic modalities in ICC. TAM interactions between tumor cells and stromal cells through protumor factors may potentiate a tumor-favorable environment including angiogenesis, matrix remodeling, tumor proliferation, and metastasis, as well as immunosuppressive effect and chemoresistance [2,6].

Past studies indicate that TAM represent a functionally heterogeneous population that can share a tumor-promoting phenotype with anti-inflammatory macrophages (MS2) [7]. However, in certain instances, they may contribute to anti-tumor effects such as cytotoxicity, NK cell activation, and phagocytosis of tumor cells, which is usually attributed to pro-inflammatory macrophages (MS1) [7,8]. Thus, it remains to be determined whether there are functionally and phenotypically distinct subsets of TAM, how they impact tumor progression, and where they are localized within the liver. Although TAM may represent a novel target for systemic immunotherapies as well as a prognostic biomarker for ICC, further research is needed to define TAM phenotypes and their correlation with biological tumor progression and clinical outcomes.

In this study, we integrated single-cell RNA sequencing (scRNA-seq) and bulk RNA sequencing (bulk RNA-seq) to analyze the diverse landscape of TAM as well as pro-inflammatory (MS1) and anti-inflammatory (MS2) macrophages in liver samples from patients with ICC and healthy liver donors [6,9]. Our analysis demonstrated the phenotypic heterogeneity of TAM, but also defined TAM-specific gene markers, TREM2, CD9, and PRMT10. To better understand the immune context of TAM, we further utilized CIBERSORT, an immune cell deconvolution algorithm, to define the immunoprofile of ICC and normal liver. Finally, using defined TAM-associated markers, we studied protein–protein interactions in STRING database analysis defining potential targets (TREM2 and LGALS3) for anti-tumor therapies in TAM activation pathways.

2. Materials and Methods

2.1. Patients and Tissue Specimens

The current analysis uses previously published scRNA-seq data that were derived from biopsy specimens from patients with ICC and healthy donors [9,10]. Data from scRNA-seq were corroborated to previously published bulk RNA-seq data that were derived from biopsy specimens from patients with ICC [11]. The datasets are publicly available on Gene Expression Omnibus (GEO) (GSE138709, GSE136103, GSE107943). Specimen collection was performed in accordance with approved protocols by the institutional review boards of treatment centers involved in acquisition of biopsies and relevant patient information as documented in original publications of datasets [9–11]. The original manuscripts that reported publicly available data that was used in this study describe methodology of

specimen processing, the reagents and manufacturers of the regents, and the kits and instruments [9–11]. The inclusion criteria were (1) ICC samples and adjacent non-tumorous tissue (ANT) from adults of both sexes for study group, (2) healthy donor tissue from adults of both sexes for control group, (3) histological confirmation of ICC and ANT in study group and healthy normal liver tissue in control group. Patient characteristics and tumor pathology are reported in Table 1 for scRNAseq data and Supplementary Table S1 for bulk RNAseq data.

Table 1. Patient characteristics.

Intrahepatic Cholangiocarcinoma Dataset (GEO GSE138709)						
Patient ID	Sex	Tumor Grade	TNM staging	Virus Infection	Pathology	Sample GEO ID
18	F	Poorly differentiated, Grade III	T3N1MX	HBV+	ICC tumor	GSM4116580
20	F	Moderately differentiated, Grade II	T2NXMX	--	ICC tumor	GSM4116581
23	M	Poorly differentiated, Grade III	T2NXMX	HBV+	ICC tumor	GSM4116583
24_1 *	M	Moderately differentiated, Grade II	T2N0M0	--	ICC tumor	GSM4116584
24_2 *	M	Moderately differentiated, Grade II	T2N0M0	--	ICC tumor	GSM4116585
18	F	Poorly differentiated, Grade III	T3N1MX	HBV+	ICC adjacent	GSM4116579
23	M	Poorly differentiated, Grade III	T2NXMX	HBV+	ICC adjacent	GSM4116582
25	M	Poorly differentiated, Grade III	T4N1M0	--	ICC adjacent	GSM4116586
Healthy Liver Dataset (GEO GSE136103)						
Healthy1_Cd45+	M	--	--	--	Normal liver	GSM4041150
Healthy1_Cd45-A						GSM4041151
Healthy1_Cd45-B						GSM4041152
Healthy2_Cd45+	M	--	--	--	Normal liver	GSM4041153
Healthy2_Cd45-						GSM4041154
Healthy3_Cd45+	M	--	--	--	Normal liver	GSM4041155
Healthy3_Cd45-A						GSM4041156
Healthy3_Cd45-B						GSM4041157
Healthy4_Cd45+	F	--	--	--	Normal liver	GSM4041158
Healthy4_Cd45-						GSM4041159

Abbreviations: M, Male; F, Female; TNM, Tumor Node Metastasis; HBV+, Hepatitis B positive; ICC, Intrahepatic cholangiocarcinoma; * Repeat biopsy of the same patient.

2.2. Single-Cell RNA-seq Quality Control and Data Processing

Single-cell RNA-seq data of five ICC samples and three adjacent tissue samples were obtained from the GSE138709 dataset and four healthy liver samples from the GSE136103. Cells that expressed fewer than 200 genes and >15% mitochondrial counts were removed. Data from both datasets were combined and analyzed in Google Colab (python version 3.10.12) using Single-Cell Analysis in Python (scanpy) package [12]. Data were normalized (scanpy: normalized_total), log+1 corrected (scanpy: log1p) and highly variable genes identified (scanpy: highly_variable_genes). Dimensional reduction analysis was performed (scanpy: pca, neighbors, umap). Batch correction between the datasets was carried out using the bbknn python package, which computed the batch balanced neighbors (scanpy: bbknn) [13] (Figure 1A, Supplementary Figure S1). Uniform Manifold Approximation and Projection (UMAP) calculations were updated, and clustering performed using the Leiden graph-clustering method [14].

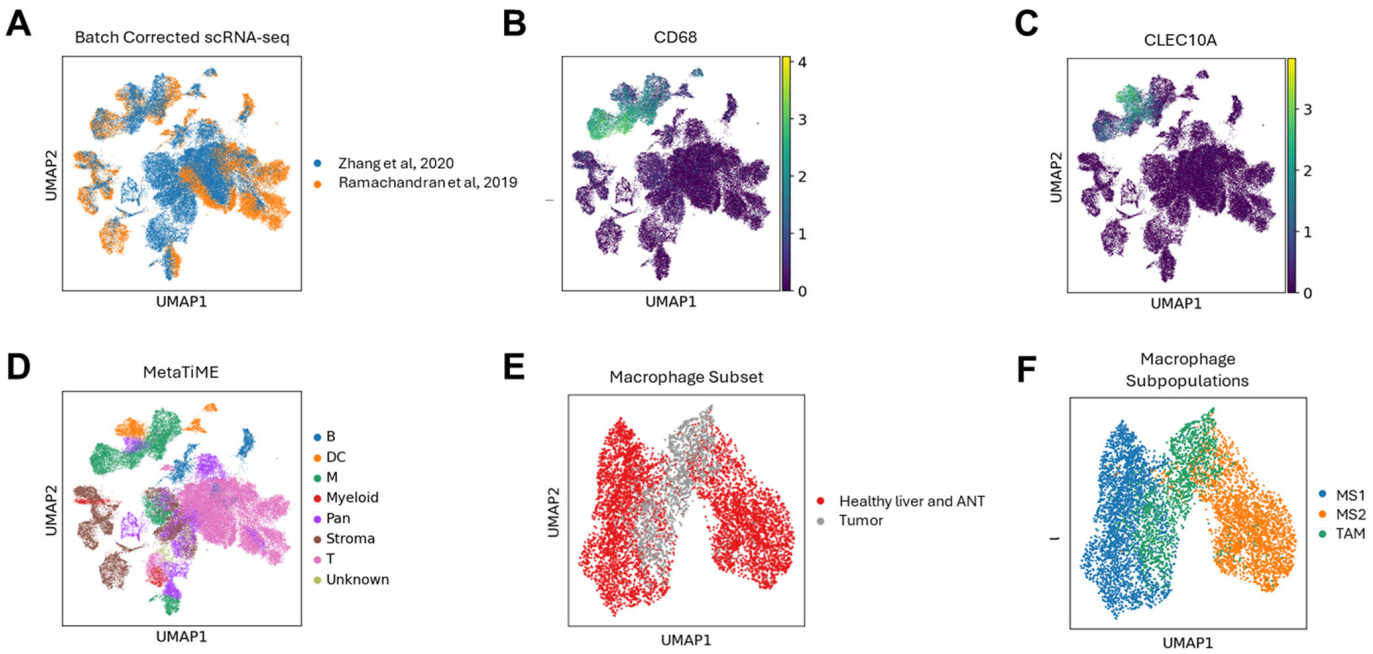

Figure 1. scRNA-seq analysis identifies three distinct macrophage subpopulations. (**A**) Merged Uniform Manifold Approximation and Projection (UMAP) plot following batch correction for 5 intrahepatic cholangiocarcinoma (ICC) samples, 3 adjacent non-tumorous tissue (ANT) samples (Zhang et al. [9]), and 4 healthy liver samples (Ramachandran et al. [10]). (**B**) Expression of the macrophage marker CD68 on the merged UMAP plot. (**C**) Expression of the dendritic cell marker CLECL10A on the merged UMAP plot. (**D**) MetaTiME annotation of major cell types in the merged UMAP plot. (B, B-cell; DC, dendritic cell; M, macrophage; Pan, pan-cancer; Stroma, stromal cell; T, T-cell) (**E**) Subset of identified macrophage cells from the merged UMAP plot: macrophages in healthy liver and ANT (red), macrophages in tumor samples (gray). (**F**) Characterization of the macrophage subset UMAP plot into three distinct populations: Macrophage Subpopulation 1 (MS1) (blue), Macrophage Subpopulation 2 (MS2) (orange), and Tumor-Associated Macrophages (TAM) (green).

2.3. Analysis of Macrophage Clusters

Macrophage cells from the batch corrected data were extracted using two sequential methods: computationally via MetaTiME cell type auto annotation algorithm and confirmed by manually visualizing known gene markers (macrophagesCD68+, dendritic-CLEC10A+) [15] (Figure 1B,C). The MetaTiME pipeline was obtained from Omicverse a python package that consists of several scRNA-seq analysis tools including the MetaTiME pipeline. MetaTiME, an auto cell type annotation method that integrates a million single cells from scRNAseq library of tumors (omicverse: ov.single.MetaTiME) was used to annotate type M cells (macrophage/monocyte) (Figure 1D). Type M cell origin was confirmed manually through the UMAP plot, defining macrophage as MCD68+/CLECL10A−. M cells were subsetted and reclustered from normal and tumor samples; neighborhood and UMAP calculations were updated (Figure 1E, Supplementary Figure S2). All macrophages in tumor samples were defined as tumor-associated macrophages (TAM). Macrophage subpopulations (MS) in normal liver (adjacent and healthy donors) were defined based on known gene markers for M1 (S100A8, LYZ, CSTA, and CD74) and M2 (CD5L, MARCO, VSIG4, and CD163) macrophages (MS1, MS2) (Figure 1D).

2.4. Identification of Unique Gene Markers in Macrophage Subpopulations

Differential gene expression analysis of scRNAseq data was performed in defined MS using the rank_gene_groups function in scanpy. The top 30 ranked genes for each

MS were visualized as a dot plot (Figure 2A–C). Differentially expressed genes (DEGs) were defined as p-value < 0.05 and log2fold change (>1, <−1). We have confirmed our results by re-analyzing the data using false discovery rate (FDR) correction (Benjamini–Hochberg method). Our results remained consistent with significant upregulation of top 30 ranked genes.

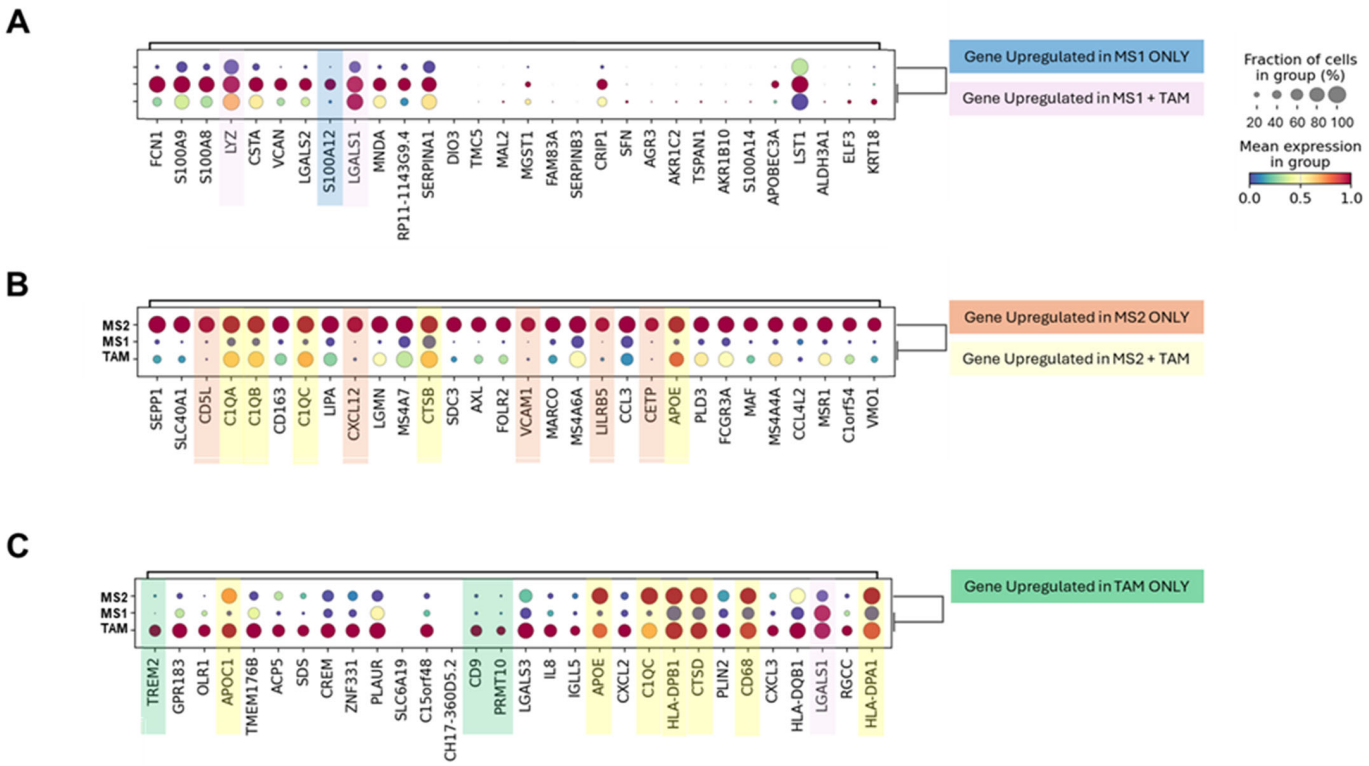

Figure 2. Top 30 upregulated differentially expressed genes (DEGs) in distinct macrophage subpopulations. The dot plot visualizes the top-ranked genes for a given group, where dot size represents the fraction of cells expressing the gene (%) and dot color indicates mean expression level between the groups. The dot plot highlights the top 30 upregulated DEGs in (**A**) MS1; genes uniquely upregulated in MS1 (blue), genes upregulated in MS1 + TAM (pink) (**B**) MS2; genes uniquely upregulated in MS2 (orange); genes upregulated in MS2 and TAM (yellow), and (**C**) TAM; genes uniquely upregulated in TAM (green).

2.5. Bulk RNA-seq Analysis

Bulk RNA-seq data for ICC (n = 27) and matched ANT (n = 27) were obtained from the GEO dataset (GSE107943). The RNA-seq data raw counts (55,770 genes in 54 samples) were processed and analyzed with the R software (version 4.2.3). First, genes with expression value less than 20 across all samples were removed. The remaining 35,898 genes were analyzed using the DESeq2 package and differentially expressed genes (DEGs) were calculated, defined as genes with an adjusted p-value <0.01 and a log2-fold change >1 or <−1. The raw counts were normalized using the DESeq2 package and used to construct heatmaps with the heatmap.2 function from the gplots package.

2.6. Corroboration of scRNA-seq and Bulk RNA-seq Data

The top 30 DEGs for MS1, MS2, and TAM from the scRNA-seq analysis were filtered if they had a mean expression greater than 0.1 in the scRNA-seq data and were present in the bulk RNA-seq DEG list. The filtered DEGs were then graphed as a heatmap using the DESeq2 normalized counts (Figure 3A–C).

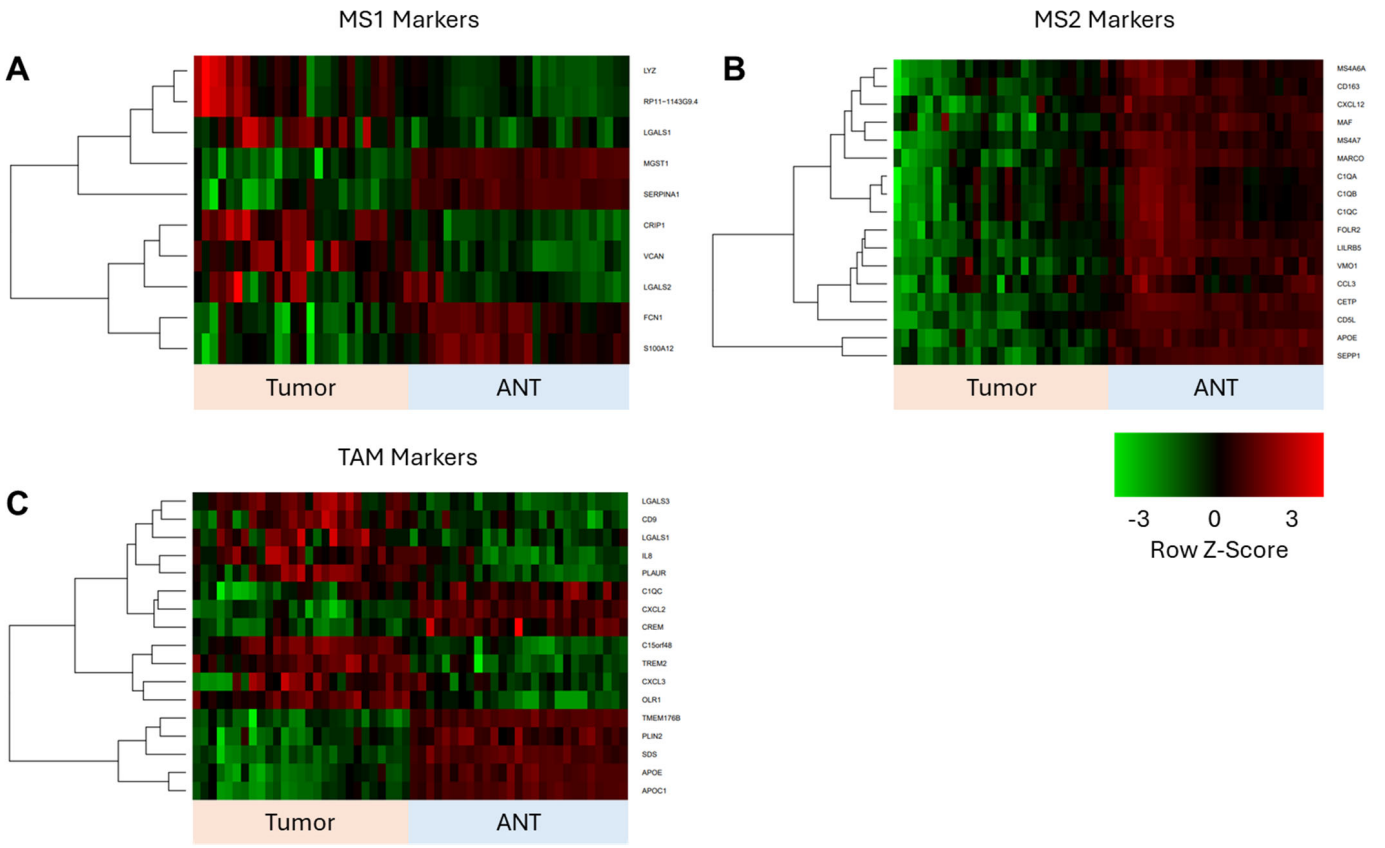

Figure 3. Validation of macrophage subpopulation (MS) gene markers identified from scRNA-seq analysis using bulk RNA-seq data from the ICC validation cohort. The top 30 upregulated genes from the scRNA-seq analysis for (**A**) MS1, (**B**) MS2, and (**C**) TAM are validated against DEGs from bulk RNA-seq data (ICC (tumor), n = 27; matched adjacent non-tumorous tissue (ANT), n = 27), with criteria of an adjusted p-value < 0.01 and a log2-fold change >1 or <−1. Genes that overlap between the scRNA-seq marker list and Bulk RNA-seq DEGs are presented as a heatmap.

2.7. CIBERSORT Analysis

Using CIBERSORT, an immune deconvolution method, the relative abundance of 22 immune cell subtypes was estimated in bulk RNA-seq of ICC tumor and ANT (Figure 4) based on a reference signature matrix of cell-type-specific gene expression. Support vector regression was used to estimate the relative proportion of each immune cell type. The "signature score" represented fraction of each immune cell subset, with the sum of all cell fractions equal to 1 for a given mixture sample. The gene counts were normalized to transcripts per million (TPM). The raw counts (35,898 genes and 54 samples) for bulk RNA-Seq data were converted to TPM. The R package Immuno-Oncology Biological Research (IOBR, ver. 0.99) in CIBERSORT pipeline was used for analysis. The statistical significance was assessed by running the algorithm 1000 times with permuted data.

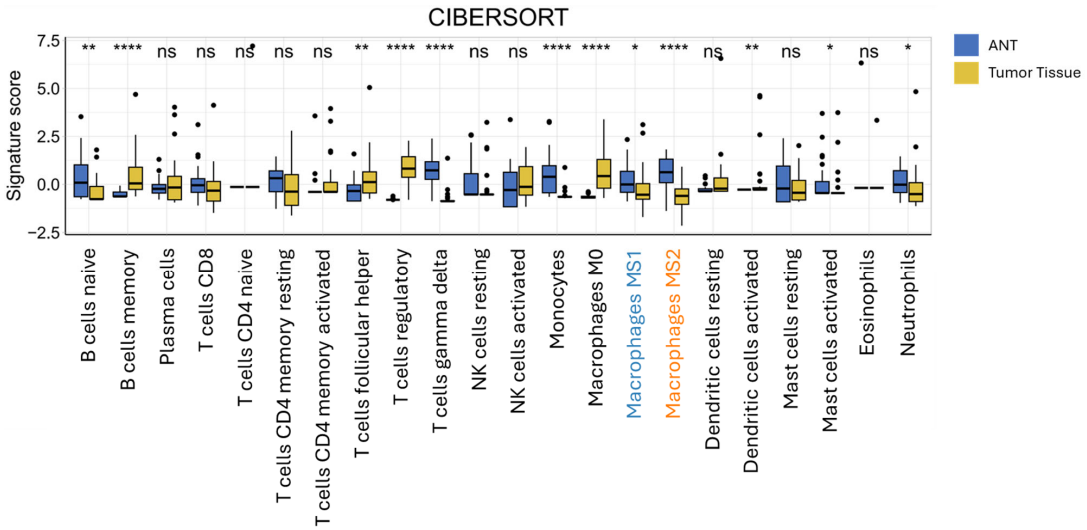

Figure 4. CIBERSORT analysis estimates the proportion of 22 immune cell types in ICC tumors and adjacent non-tumorous tissue (ANT). The estimated proportions of immune cell types are presented as box plots for ANT (blue, $n = 27$) and tumor (yellow, $n = 27$) tissue, utilizing the Immuno-Oncology Biological Research (IOBR) R package. (**** p-value < 0.0001, ** p-value < 0.01, * p-value < 0.05, and ns = not significant).

2.8. STRING Analysis

STRING database (version 12.0, https://string-db.org/, accessed on 20 January 2025) was used to study the contribution of unique TAM-related genes to networks of protein–protein interactions. The top 30 upregulated genes in TAM cohort compared to MS1 and MS2 were analyzed in the STRING database. High confidence level of 0.7 was used (Figure 5A,B).

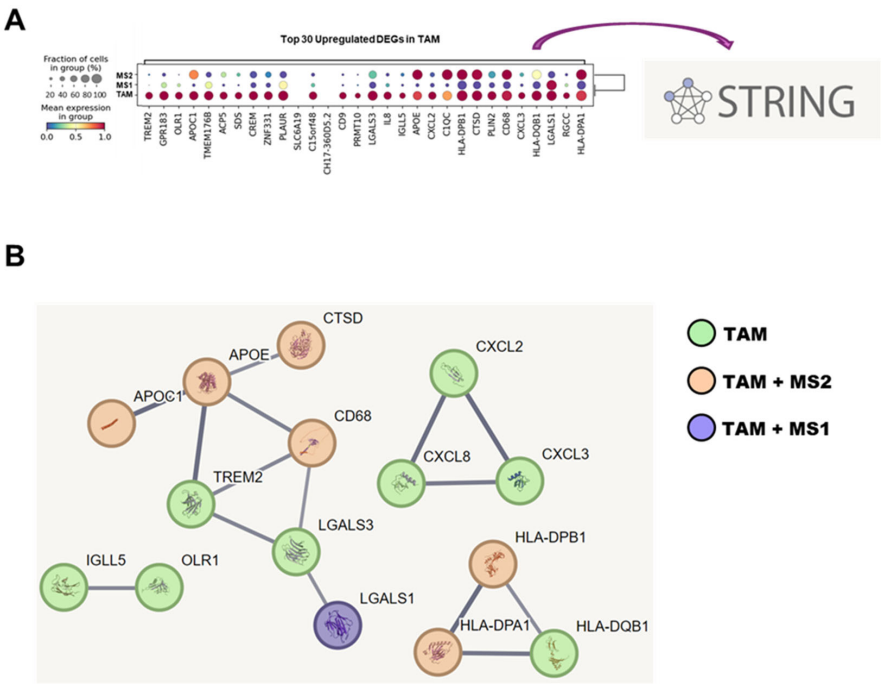

Figure 5. Protein–protein interaction networks of TAM-associated gene products. (**A**) The top 30 upregulated DEGs in TAM are analyzed using the STRING database, with their respective protein names. (**B**) A network represents TAM-associated proteins that are predicted to interact with other TAM-associated proteins (confidence level = 0.7). Proteins are color-coded: TAM-only proteins (green), both TAM and MS2 (orange), and both TAM and MS1 (purple).

2.9. Statistical Analysis

All statistical tests were performed by established R and python packages. The Wilcoxon rank sum test was used in the IOBR package for CIBERSORT analysis to compare tumor and normal tissue groups. A p-value < 0.05 was considered significant. DESeq2 package was used to calculate DEGs in tumor and normal tissue groups. A log2-fold change >1 or <−1 and adjusted p-value < 0.01 was considered significant.

3. Results

3.1. Patient Characteristics

For scRNA-seq analysis, ICC samples and adjacent tissue from five patients and healthy liver from four donors were used. In the scRNA-seq ICC cohort, 60% were female, and 40% of patients were hepatitis B positive (HBV+). A total of 40% of tumors were characterized as moderately differentiated and 60% of tumors were poorly differentiated. In scRNA-seq healthy liver cohort, 50% were female (Table 1). For bulk RNA-seq data that was used for corroboration of results, ICC samples, and adjacent matched tissue from 31 patients were used. In the bulk RNA-seq ICC cohort, 29% were female, 13% were HBV+, and 58% of tumors were characterized as moderately and 35% as poorly differentiated, with 2 tumors not classified (Supplementary Table S1).

3.2. Characterization of Macrophage Subpopulations by scRNA-seq Data

Analysis of scRNA-seq data included 64,554 cells (17,090 tumor cells; 47,464 normal cells) that were derived from five ICC patients and four healthy liver donors. Of 64,554 cells, 60,619 cells passed quality control. The batch effect was initially observed between the two datasets (Supplementary Figure S1). After batch correction, cells were evenly distributed between two datasets (Figure 1A). Macrophages were identified based on overexpression of *CD68* (a macrophage marker) (Figure 1B) and absence of *CLECL10A* expression (a dendritic cell marker) (Figure 1C) and confirmed through MetaTiME annotation of cell types, where M annotates macrophage/monocyte (Figure 1D). A total of 7180 $M^{CD68+/CLECL10A-}$ cells were identified, subsetted, and reanalyzed. Macrophages from ICC tumor tissue samples, tumor-derived macrophages (TAM), formed a distinct cluster on UMAP plot (Figure 1E). Two macrophage subpopulations were present and evenly overlapping in ANT and healthy normal tissue, MS1 ($M^{FCN1+/S100A8+/LYZ+/CSTA+}$, i.e., pro-inflammatory macrophages) and MS2 ($M^{SEPP1+/CD5L+/MARCO+/CD163+}$, i.e., anti-inflammatory macrophages) (Figure 1F, Supplementary Figure S2).

3.3. TAM Population Is Characterized by Expression of TREM2, CD9 and PRMT10

The top 30 DEGs in individual subpopulations of interest MS1, MS2, and TAM were examined (Figure 2A–C and Supplementary Figure S3). The fold changes in the top 30 DEGs are reported in Supplementary Table S3. S100A12 was the only of one of the top 30 DEGs that was upregulated in the MS1 subpopulation alone, which is consistent with the pro-inflammatory phenotype of these cells, whereas LYZ and LGALS1 were upregulated in both MS1 and TAM, suggesting macrophage plasticity toward tumor-associated phenotype (Figure 2A). CD5L, CXCL12, VCAM1, LILRB5, and CETP were uniquely upregulated in the MS2 subpopulation, whereas C1QA, C1QB, C1QC, CTSB, APOE, APOC1, HLA-DPB1, CTSD, CD68, and HLA-DPA1 were overexpressed in MS2 and TAM subpopulations (Figure 2B,C). TREM2, CD9, and PRMT10 were present only in the TAM phenotype with prevalence of expression in 40–60% of TAM per sample (Figure 2C). In summary, the MS1 subpopulation was primarily characterized by the upregulation of genes in the pro-inflammatory cascade, although LGALS1 has a more complex role. Depending on the context, LGALS1 has anti- and pro-inflammatory properties in addition to inducing

macrophage reprogramming and promoting the TAM phenotype [16,17]. Upregulation of CD5L, CXCL12, LILRB5, and CETP expression supported the anti-inflammatory and tolerogenic phenotype of MS2 subpopulation [18], whereas the unique expression of TREM2, CD9, and PRMT10 by TAM suggested an anti-inflammatory and pro-oncogenic phenotype (Supplemental Table S2) [18]. The variable expression of TREM2, CD9, and PRMT10 by TAM indicated the heterogenous nature of TAM subpopulations.

3.4. Corroboration of scRNAseq Data with Bulk RNAseq Data from ICC Validation Cohort

S100A12 that was solemnly expressed by MS1 in the top 30 DEGs from scRNAseq analysis was uniquely upregulated in ANT from bulk RNAseq analysis. In contrast, the expression of LYZ and LGALS1, shared markers of MS1 and TAM from scRNAseq analysis, was primarily limited to tumor tissue (Figure 3A). Remarkably, unique markers of MS2 as well as those shared between MS2 and TAM based on scRNAseq data were diminished in bulk RNAseq analysis of ICC and uniformly upregulated in ANT (Figure 3B). TREM2 and CD9 gene signature of TAM from scRNAseq analysis was primarily upregulated in tumors and downregulated in ANT from bulk RNAseq analysis (Figure 3C). Overall, the findings of scRNAseq analysis were supported by bulk RNAseq analysis of ICC and ANT.

3.5. CIBERSORT Immune Cell Deconvolution of Bulk RNAseq Data from ICC and Adjacent Non-Tumorous Tissue

Based on bulk RNAseq analysis, immune cell populations that were upregulated in ICC in comparison to ANT included B memory cells; activated T memory, T follicular helper and T regulatory cells; and M0 macrophages and activated dendritic cells. Downregulated immune cell populations in ICC in comparison to ANT included naïve B cells, gamma delta T cells, monocytes, activated mast cells, neutrophils, MS2 macrophages, and to a lesser extent MS1 macrophages (Figure 4). The pattern of upregulated immune cell populations in ICC suggested the trigger of adoptive immune response with a particular increase in Treg population.

3.6. STRING Database Analysis of TAM-Associated Genes in Network of Protein–Protein Interactions

Of the top 30 upregulated DEGs in TAM, STRING database analysis demonstrated four protein–protein networks that involved TAM-specific genes, including the following: TREM2-LGALS3, OLR1-IGLL5, CXCL2-CXCL3-CXCL8, and HLA-DQB1 (Figure 5A,B). The largest network that included TREM2 and LGALS3 demonstrated close interaction with APOC1, APOE, CTSD, and CD68 gene products that are overexpressed in TAM and MS2 as well as interaction with LGALS1, which is overexpressed in TAM and MS1 (Figure 5).

4. Discussion

ICC remains one of the most lethal primary liver malignancies, with limited therapeutic options and poor immunotherapy responsiveness [1,3,4]. A defining feature of ICC is its immunologically "cold" TME, which exhibits extensive desmoplasia, widespread immunosuppressive signaling, and sparse cytotoxic immune cell infiltration [19]. Notably, CD8+ T cells and natural killer (NK) cells are underrepresented in ICC lesions, whereas innate immune cells especially TAM and myeloid-derived suppressor cells (MDSCs) are markedly enriched [20]. Macrophages within the TME exhibit extraordinary plasticity, toggling between pro-inflammatory and anti-inflammatory states in response to environmental signals such as cytokines, hypoxia, and metabolic stress [21]. In ICC, TAM are not only abundant but have been strongly associated with poor prognosis, immune evasion, and resistance to treatment [22,23]. However, much remains unclear about their phenotypic diversity in ICC, especially given the limitations of the traditional M1/M2 polarization framework. This binary model inadequately captures the nuance of macrophage behavior in cytokine-rich

environments like ICC. Therefore, a granular, high-resolution transcriptional atlas of TAM in ICC is essential to uncover their pathogenic roles and therapeutic vulnerabilities.

To define the phenotypic landscape of macrophages in ICC, we integrated scRNAseq of over 60,000 cells derived from ICC tumors, adjacent tissue, and healthy donor livers. From this dataset, we identified three dominant macrophage populations: a pro-inflammatory MS1 subset (MFCN1$^+$/S100A8$^+$/LYZ$^+$), an anti-inflammatory MS2 subset (MCD5L$^+$/CD163$^+$/MARCO$^+$), and a tumor-specific TAM population confined to tumor tissue. On UMAP visualization, TAM occupied an intermediate position between MS1 and MS2 clusters (Figure 1F), suggesting a transcriptionally hybrid population [24]. Co-existence of pro-inflammatory and anti-inflammatory features in TAM may be beneficial to tumor progression and survival. Pro-inflammatory components contribute to chronic inflammation and angiogenesis promoting tumor proliferation whereas anti-inflammatory components facilitate immunosuppressive TME impairing anti-tumor immune response and destruction.

DEG analysis, visualized by dot plots (Figure 2A–C), revealed both distinct and shared transcriptional signatures across macrophage subsets. The MS1 subset was characterized by distinct upregulation of S100A12, a calcium-binding alarmin implicated in acute inflammatory responses [25,26]. Meanwhile TAM shared other markers with MS1, including LYZ, an antimicrobial effector [27], and LGALS1, a lectin involved in modulating immune cell interactions [28]. This pattern suggests that TAM partially retain inflammatory profile during their transcriptional reprogramming within the TME.

Conversely, MS2 macrophages displayed distinct enrichment of CD5L (lipid scavenging) [29,30], CXCL12 (chemotaxis) [31,32], VCAM1 (adhesion) [33], LILRB5 (inhibitory immune checkpoint) [34], and CETP (cholesterol transfer) [35], representing a tissue-reparative and immunoregulatory program [36]. TAM also demonstrated partial upregulation of MS2-associated genes supporting lipid metabolism [37], proteolysis [38], and antigen processing such as C1QA, C1QB, C1QC (complement components aiding apoptotic clearance) [39,40], CTSB and CTSD (lysosomal proteases involved in extracellular matrix degradation) [41–44], APOE and APOC1 (apolipoproteins supporting cholesterol efflux under hypoxia) [45–47], CD68 (phagocytic marker) [48], and MHC class II genes HLA-DPB1 and HLA-DPA1, indicating retention of antigen-presenting competency [49–51]. This pattern suggests that although TAM lose many classical tissue-repairing features associated with MS2 macrophages, they selectively retain metabolic and antigen-processing functions necessary for survival within the hostile TME. Rather than fully adopting a reparative identity, TAM appear transcriptionally adapted to balance immune modulation, matrix remodeling, and metabolic stress responses, features that collectively support tumor progression and immune suppression [52,53].

Despite these shared features, subpopulation of TAM displayed a transcriptionally unique signature, marked by exclusive expression of TREM2 (lipid sensing and immune checkpoint control) [54], CD9 (exosomal trafficking and cellular adhesion), and PRMT10 (epigenetic regulation via histone methylation) (Figure 2C). These genes were not significantly expressed in MS1 or MS2 subsets, highlighting a TAM-specific transcriptional reprogramming aligned with the metabolically stressed and immunosuppressive TME. The unique expression of TREM2 in TAM subpopulations is not exclusive to ICC. In hepatocellular carcinoma, the most common liver malignancy in adults, the presence of heterogenous TAM subpopulations that are rich in TREM2 was associated with poor patient prognosis [55], whereas in hepatoblastoma, the most common pediatric liver malignancy, the heterogeneity of TAM subpopulations has not been well defined [56].

To corroborate these findings, we validated the scRNA-seq signatures in an independent bulk RNA-seq cohort of ICC tumors and adjacent tissues. Shared genes of MS1 and

TAM, initially enriched in normal liver macrophages at the single-cell level, showed overexpression in tumor, whereas S100A12, unique to MS1, was primarily upregulated in ANT (Figure 3A), indicating the pro-inflammatory state of ANT in patients with ICC. MS2 signatures, however, were substantially diminished in tumors but retained in adjacent tissues (Figure 3B), consistent with suppression of tissue-repair macrophage signatures within the TME. Two unique TAM-associated genes, TREM2 and CD9, were expressed in the majority of tumor samples compared to normal adjacent tissue. However, gene signature, which was shared by TAM and MS2, demonstrated partial expression in both tumors and adjacent tissues (Figure 3C), suggesting transcriptional overlap and early immune remodeling in peritumoral regions. Collectively, these findings indicate that TAMs in ICC arise through selective transcriptional reprogramming, preserving elements of both inflammatory and anti-inflammatory macrophage programs while adapting to tumor-derived cues [57]. This process generates a metabolically adaptive, immunosuppressive hybrid state that facilitates immune evasion, matrix remodeling, and tumor progression. Critically, the reproducibility of these signatures across scRNA-seq and bulk RNA-seq datasets support their potential as biomarkers or therapeutic targets.

To further characterize the immune architecture of the ICC TME, we performed CIBERSORT-based immune cell deconvolution on bulk RNA-seq data from ICC tumors and matched adjacent tissue (Figure 4). Immune deconvolution revealed a marked depletion of MS2 macrophages and, to a lesser extent, a reduction in MS1 macrophages within tumor samples, consistent with our scRNA-seq findings. This pattern reinforces the concept that TAM in ICC selectively lose tissue-repairing (MS2) transcriptional programs while partially retaining inflammatory (MS1) features. Notably, this shift was accompanied by a pronounced increase in M0 macrophages—an undifferentiated macrophage state characterized by the absence of canonical M1 or M2 polarization signatures. The enrichment of M0 macrophages may reflect a population of transitional or incompletely polarized macrophages, or alternatively, hybrid TAM phenotypes that co-express elements of both MS1- and MS2-like programs without full commitment to either lineage. It is important to note, however, that the CIBERSORT algorithm does not explicitly define TAM as a distinct immune subset, and thus the observed M0 expansion may in part reflect the transcriptional complexity of TAM that fall outside traditional polarization categories. Interestingly, additional CIBERSORT analysis demonstrated distinct changes in the adaptive immunoprofile of TME compared to ANT, including the depletion of naïve B cells and gamma delta T cells, with an increase in memory B cells and T-regulatory cells, suggesting a partially immunosuppressive state.

Our study also explored the potential protein networks that are involved in TAM-associated pathways. STRING-based protein–protein interaction (PPI) network analysis of the top 30 upregulated DEG in TAM revealed four major clusters (Figure 5A,B). The largest and most functionally coherent cluster was supported by TREM2 and LGALS3, two genes selectively upregulated in TAM compared to MS1 and MS2 macrophages [58,59]. This cluster incorporated critical metabolic and immunoregulatory proteins, APOE, APOC1, CTSD, CD68, and LGALS1, suggesting that TAM orchestrate the survival of lipid metabolism, lysosomal function, and antigen processing pathways in the desmoplastic TME of ICC [18].

TREM2, a type I transmembrane receptor primarily expressed by myeloid cells, regulates macrophage survival, apoptotic debris clearance, and adaptation to hypoxic environments [58,60,61]. TREM2$^+$ macrophages have been widely implicated in promoting immunosuppression across solid tumors, including lung, liver, breast, and pancreas cancers [58]. Specifically, in hepatocellular carcinoma, TREM2$^+$ TAM suppressed CD8$^+$ T cell infiltration by downregulating CXCL9 and promoting galectin-1 (LGALS1) secretion,

resulting in impaired cytotoxic immune surveillance. In our study, immune deconvolution revealed significant upregulation of Tregs but no corresponding increase in $CD8^+$ T cells within ICC tumors (Figure 4), aligning with previous reports linking TREM2 activity to global immune dysfunction and T cell suppression.

The therapeutic relevance of TREM2 is increasingly recognized. In colorectal cancer, a recent study demonstrated that targeting TREM2 protein using a PD-1-TREM2 single-chain variable fragment (scFv) enhanced anti-tumor efficacy by simultaneously blocking PD-1/PD-L1 signaling and neutralizing TREM2-mediated immunosuppression, thereby restoring $CD8^+$ T cell effector functions [62].

Importantly, our findings highlight a functional interplay between TREM2 and LGALS3. Recent studies in lung cancer demonstrated that LGALS3 stabilizes $TREM2^+$ macrophages, skewing them toward an M2-like, immunosuppressive phenotype with reduced antigen-presenting and co-stimulatory capacity [63]. Notably, dual targeting of LGALS3 inhibition (e.g., with GB1107) and TREM2 blockade synergistically inhibited tumor progression and reduced infiltration of immunosuppressive macrophages [63]. Since we observed the upregulation of TREM2 and LGALS3 in our study, targeting the TREM2–LGALS3 axis in ICC could modulate TAM away from tumor-supportive states and restore anti-tumor immunity.

CD9 and PRMT10 were also identified in the top 30 upregulated genes that characterized TAM [64,65]. However, no protein–protein networks were identified for these genes. This may be attributed to high confidence score of 0.7 that was used to identify biologically meaningful networks and decrease false positive rate of discovery.

Our study has several limitations that should be considered when interpreting the findings. The single-cell analysis was derived from a small number of ICC and healthy donor samples, which may not fully capture the diversity of macrophage phenotypes across patient populations [66]. Further, the study utilized two publicly available datasets for scRNA-seq data that required batch correction to accommodate for systematic technical variation introduced by differences in techniques. The bulk RNA-seq validation cohort was retrospectively assembled, and detailed clinical information such as prior adjuvant chemotherapy, exposure to immunosuppressive agents, or other relevant treatments were unavailable, potentially confounding transcriptomic comparisons. Our interpretations are based on transcriptional data, and the functional properties of these subsets, particularly the TREM2–LGALS3-associated TAM population, should be validated through protein level analysis and dedicated mechanistic studies. In the present study, we focused on the top DEGs in MS1, MS2, and TAM subpopulations. It is possible that other DEGs with a lower expression fold may significantly contribute to TAM phenotype and may serve as potential prognostic and therapeutic targets. Although the CIBERSORT algorithm allowed us to compare the immune cell populations between TME and matched ANT, it did not have specific definition of TAM, thus limiting our analysis. We plan to further investigate the correlation between different immune cell populations in the follow-up study with our own data. The current study is limited by the analysis of the retrospectively collected information from the publicly available data. It has been demonstrated that increasing the burden of TAM in thyroid, lung, and breast cancer is associated with poor survival [22]. Due to the limited availability of clinical data, the survival analysis was not performed.

5. Conclusions

This study provides a comprehensive, high-resolution map of macrophage heterogeneity in intrahepatic cholangiocarcinoma, identifying a tumor-specific TAM population that diverges from classical M1 and M2 polarization states. Rather than preserving full tissue-repairing (MS2-like) or inflammatory (MS1-like) programs, TAM display a hybrid

immunometabolic phenotype, selectively incorporating and reprogramming elements of both lineages. Even within the TAM population, unique gene signature was heterogeneous as demonstrated in dot plot analysis of gene expression and percent cell affected (Figure 2C). Further mechanistic studies are needed to discern whether TMA represent a transitional or separate populations of macrophages.

Integrated single-cell and bulk RNA sequencing, corroborated by immune deconvolution, demonstrated a selective loss of MS2-associated tissue-repair signatures and the emergence of transcriptionally intermediate macrophage states within the TME. The TREM2–LGALS3 axis was a dominant protein network that was identified based on DEGs of TAM.

Rather than advocating for indiscriminate macrophage depletion, which risks compromising essential immune and tissue functions, these findings support a therapeutic model based on macrophage heterogeneity. Understanding the factors that drive macrophage reprogramming and possibly targeting regulators such as TREM2 and LGALS3 may offer new strategies to dismantle immune resistance and restore anti-tumor immunity in ICC. However, the solution of targeting TREM2-LGALS3 axis may achieve only partial therapeutic success given the heterogeneity of TREM2 expression in TAM subpopulations.

Supplementary Materials: The following supporting information can be downloaded at https://www.mdpi.com/article/10.3390/livers5040053/s1: Figure S1: UMAP plot before batch correction; Figure S2: UMAP plot illustrating macrophage cell subsets; Figure S3: Gene upregulation in MS1, MS2, TAM; Table S1: Patient characteristics; Table S2: Functional Characteristics of Gene Products; Table S3: Top DEGs in MS1, MS2, and TAM.

Author Contributions: Conceptualization, J.S.B. and V.A.K.; methodology, J.S.B. and V.A.K.; validation, J.S.B. and V.A.K.; formal analysis, J.S.B.; resources, M.L.M.; writing—original draft preparation, J.S.B. and V.A.K.; writing—review and editing, O.M.M., S.M.K., R.M.L., A.R., and D.J.D.; supervision, V.A.K.; funding acquisition, V.A.K. All authors have read and agreed to the published version of the manuscript.

Funding: This research was funded by National Institute on Aging, grant number K08 AG068374 NIA.

Institutional Review Board Statement: Ethical review and approval were waived according to U.S. 45 CFR 46.102 because the data available to the public are not individually identifiable and therefore analysis did not involve human subjects.

Informed Consent Statement: The current study was performed using publicly available data from the Gene Expression Omnibus data portal (https://www.ncbi.nlm.nih.gov/geo/, accessed on 20 December 2024). Therefore, no human subject consent was required.

Data Availability Statement: The datasets analyzed for this study were acquired from the Gene Expression Omnibus data portal (https://www.ncbi.nlm.nih.gov/geo/, accessed on 20 December 2024).

Conflicts of Interest: The authors declare no conflicts of interest. The funders had no role in the design of the study; in the collection, analyses, or interpretation of data; in the writing of the manuscript; or in the decision to publish the results.

Abbreviations

ANT	adjacent non-tumorous tissue
APOC1	apolipoprotein C1
APOE	apolipoprotein E
C1QA	complement C1q A chain
C1QB	complement C1q B chain
C1QC	complement C1q C chain
CD5L	CD5 antigen-like

CETP	cholesteryl ester transfer protein
CLEC10A	C-type lectin domain family 10 member A
CSTA	cystatin A
CTSB	cathepsin B
CTSD	cathepsin D
CXCL2	C-X-C motif chemokine ligand 2
CXCL3	C-X-C motif chemokine ligand 3
CXCL8	C-X-C motif chemokine ligand 8
CXCL12	C-X-C motif chemokine ligand 12
DEGs	differentially expressed genes
FCN1	ficolin 1
GEO	gene expression omnibus
HBV+	hepatitis B positive
HLA-DPA1	major histocompatibility complex, class II, DP alpha 1
HLA-DPB1	major histocompatibility complex, class II, DP beta 1
HLA-DQB1	major histocompatibility complex, class II, DQ beta 1
ICC	intrahepatic cholangiocarcinoma
IGLL5	immunoglobulin lambda like polypeptide 5
IOBR	immuno-oncology biological research
LGALS1	galectin-1
LGALS3	galectin-3
LILRB5	leukocyte immunoglobulin-like receptor subfamily B member 5
LYZ	lysozyme
MARCO	macrophage receptor with collagenous structure
MDSCs	myeloid-derived suppressor cells
MS	macrophage subpopulations
MS1	inflammatory macrophages
MS2	anti-inflammatory macrophages
NK	natural killer
OLR1	oxidized low density lipoprotein receptor 1
OS	overall survival
PPI	protein–protein interaction
PRMT10	protein arginine methyltransferase 10
S100A8	S100 calcium-binding protein A8
S100A12	S100 calcium-binding protein A12
ScRNA-seq	single-cell rna sequencing
SEPP1	selenoprotein P, plasma, 1
TAM	tumor-associated macrophages
TME	tumor microenvironment
TPM	transcripts per million
T reg	regulatory T-cells
TREM2	triggering receptor expressed on myeloid cells 2
UMAP	uniform manifold approximation and projection
VCAM1	Vascular Cell Adhesion Molecule 1

References

1. Olthof, P.B.; Franssen, S.; van Keulen, A.-M.; van der Geest, L.G.; Hoogwater, F.J.; Coenraad, M.; van Driel, L.M.; Erdmann, J.I.; Mohammad, N.H.; Heij, L.; et al. Nationwide treatment and outcomes of intrahepatic cholangiocarcinoma. *HPB* **2023**, *25*, 1329–1336. [CrossRef]
2. Zhou, M.; Wang, C.; Lu, S.; Xu, Y.; Li, Z.; Jiang, H.; Ma, Y. Tumor-associated macrophages in cholangiocarcinoma: Complex interplay and potential therapeutic target. *EBioMedicine* **2021**, *67*, 103375. [CrossRef] [PubMed]
3. Saha, S.K.; Zhu, A.X.; Fuchs, C.S.; Brooks, G.A. Forty-Year Trends in Cholangiocarcinoma Incidence in the U.S.: Intrahepatic Disease on the Rise. *Oncologist* **2016**, *21*, 594–599. [CrossRef] [PubMed]

4. Tataru, D.; Khan, S.A.; Hill, R.; Morement, H.; Wong, K.; Paley, L.; Toledano, M.B. Cholangiocarcinoma across England: Temporal changes in incidence, survival and routes to diagnosis by region and level of socioeconomic deprivation. *JHEP Rep.* **2024**, *6*, 100983. [CrossRef] [PubMed]
5. Greten, T.F.; Schwabe, R.; Bardeesy, N.; Ma, L.; Goyal, L.; Kelley, R.K.; Wang, X.W. Immunology and immunotherapy of cholangiocarcinoma. *Nat. Rev. Gastroenterol. Hepatol.* **2023**, *20*, 349–365. [CrossRef]
6. Pittet, M.J.; Michielin, O.; Migliorini, D. Clinical relevance of tumour-associated macrophages. *Nat. Rev. Clin. Oncol.* **2022**, *19*, 402–421. [CrossRef]
7. Chen, F.; Sheng, J.; Li, X.; Gao, Z.; Hu, L.; Chen, M.; Fei, J.; Song, Z. Tumor-associated macrophages: Orchestrators of cholangiocarcinoma progression. *Front. Immunol.* **2024**, *15*, 1451474. [CrossRef]
8. Evans, R.; Alexander, P. Cooperation of immune lymphoid cells with macrophages in tumour immunity. *Nature* **1970**, *228*, 620–622. [CrossRef]
9. Zhang, M.; Yang, H.; Wan, L.; Wang, Z.; Wang, H.; Ge, C.; Liu, Y.; Hao, Y.; Zhang, D.; Shi, G.; et al. Single-cell transcriptomic architecture and intercellular crosstalk of human intrahepatic cholangiocarcinoma. *J. Hepatol.* **2020**, *73*, 1118–1130. [CrossRef]
10. Ramachandran, P.; Dobie, R.; Wilson-Kanamori, J.R.; Dora, E.F.; Henderson, B.E.P.; Luu, N.T.; Portman, J.R.; Matchett, K.P.; Brice, M.; Marwick, J.A.; et al. Resolving the fibrotic niche of human liver cirrhosis at single-cell level. *Nature* **2019**, *575*, 512–518. [CrossRef]
11. Ahn, K.S.; O'bRien, D.; Na Kang, Y.; Mounajjed, T.; Kim, Y.H.; Kim, T.-S.; Kocher, J.-P.A.; Allotey, L.K.; Borad, M.J.; Roberts, L.R.; et al. Prognostic subclass of intrahepatic cholangiocarcinoma by integrative molecular-clinical analysis and potential targeted approach. *Hepatol. Int.* **2019**, *13*, 490–500. [CrossRef]
12. Wolf, F.A.; Angerer, P.; Theis, F.J. SCANPY: Large-scale single-cell gene expression data analysis. *Genome Biol.* **2018**, *19*, 15. [CrossRef] [PubMed]
13. Polański, K.; Young, M.D.; Miao, Z.; Meyer, K.B.; A Teichmann, S.; Park, J.-E. BBKNN: Fast batch alignment of single cell transcriptomes. *Bioinformatics* **2020**, *36*, 964–965. [CrossRef] [PubMed]
14. Traag, V.A.; Waltman, L.; Van Eck, N.J. From Louvain to Leiden: Guaranteeing well-connected communities. *Sci. Rep.* **2019**, *9*, 5233. [CrossRef] [PubMed]
15. Zhang, Y.; Xiang, G.; Jiang, A.Y.; Lynch, A.; Zeng, Z.; Wang, C.; Zhang, W.; Fan, J.; Kang, J.; Gu, S.S.; et al. MetaTiME integrates single-cell gene expression to characterize the meta-components of the tumor immune microenvironment. *Nat. Commun.* **2023**, *14*, 2634. [CrossRef]
16. Finotto, L.; Cole, B.; Giese, W.; Baumann, E.; Claeys, A.; Vanmechelen, M.; Decraene, B.; Derweduwe, M.; Lakic, N.D.; Shankar, G.; et al. Single-cell profiling and zebrafish avatars reveal LGALS1 as immunomodulating target in glioblastoma. *EMBO Mol. Med.* **2023**, *15*, e18144. [CrossRef]
17. Yu, X.; Qian, J.; Ding, L.; Yin, S.; Zhou, L.; Zheng, S. Galectin-1: A Traditionally Immunosuppressive Protein Displays Context-Dependent Capacities. *Int. J. Mol. Sci.* **2023**, *24*, 6501. [CrossRef]
18. Information NCfB. NCBI Gene Datasets: NCBI. Available online: https://www.ncbi.nlm.nih.gov/datasets/gene/ (accessed on 20 December 2024).
19. Zhang, G.; Li, J.; Li, G.; Zhang, J.; Yang, Z.; Yang, L.; Jiang, S.; Wang, J. Strategies for treating the cold tumors of cholangiocarcinoma: Core concepts and future directions. *Clin. Exp. Med.* **2024**, *24*, 193. [CrossRef]
20. Liu, Z.-L.; Liu, X.; Peng, H.; Peng, Z.-W.; Long, J.-T.; Tang, D.; Peng, S.; Bao, Y.; Kuang, M. Anti-PD-1 Immunotherapy and Radiotherapy for Stage IV Intrahepatic Cholangiocarcinoma: A Case Report. *Front. Med.* **2020**, *7*, 368. [CrossRef]
21. Kerneur, C.; Cano, C.E.; Olive, D. Major pathways involved in macrophage polarization in cancer. *Front. Immunol.* **2022**, *13*, 1026954. [CrossRef]
22. Jung, K.Y.; Cho, S.W.; A Kim, Y.; Kim, D.; Oh, B.-C.; Park, D.J.; Park, Y.J. Cancers with Higher Density of Tumor-Associated Macrophages Were Associated with Poor Survival Rates. *J. Pathol. Transl. Med.* **2015**, *49*, 318–324. [CrossRef]
23. Li, S.; Zhang, M.; Gao, Y.; Zhao, C.; Liao, S.; Zhao, X.; Ning, Q.; Tang, S. Mechanisms of tumor-associated macrophages promoting tumor immune escape. *Carcinogenesis* **2025**, *46*, bgaf023. [CrossRef] [PubMed]
24. Mossel, D.M.; Moganti, K.; Riabov, V.; Weiss, C.; Kopf, S.; Cordero, J.; Dobreva, G.; Rots, M.G.; Klüter, H.; Harmsen, M.C.; et al. Epigenetic Regulation of S100A9 and S100A12 Expression in Monocyte-Macrophage System in Hyperglycemic Conditions. *Front. Immunol.* **2020**, *11*, 1071. [CrossRef] [PubMed]
25. Zhang, Y.; Li, Z.; Chen, C.; Wei, W.; Li, Z.; Huang, H.; Zhou, H.; He, W.; Xia, J.; Li, B.; et al. S100A12 is involved in the pathology of osteoarthritis by promoting M1 macrophage polarization via the NF-κB pathway. *Connect. Tissue Res.* **2024**, *65*, 133–145. [CrossRef] [PubMed]
26. Lira-Junior, R.; Holmström, S.B.; Clark, R.; Zwicker, S.; Majster, M.; Johannsen, G.; Axtelius, B.; Åkerman, S.; Svensson, M.; Klinge, B.; et al. S100A12 Expression Is Modulated During Monocyte Differentiation and Reflects Periodontitis Severity. *Front. Immunol.* **2020**, *11*, 86. [CrossRef]

27. Gu, Z.; Wang, L.; Dong, Q.; Xu, K.; Ye, J.; Shao, X.; Yang, S.; Lu, C.; Chang, C.; Hou, Y.; et al. Aberrant LYZ expression in tumor cells serves as the potential biomarker and target for HCC and promotes tumor progression via csGRP78. *Proc. Natl. Acad. Sci. USA* **2023**, *120*, e2215744120. [CrossRef]
28. Rudjord-Levann, A.M.; Ye, Z.; Hafkenscheid, L.; Horn, S.; Wiegertjes, R.; Nielsen, M.A.; Song, M.; Mathiesen, C.B.; Stoop, J.; Stowell, S.; et al. Galectin-1 induces a tumor-associated macrophage phenotype and upregulates indoleamine 2,3-dioxygenase-1. *iScience* **2023**, *26*, 106984. [CrossRef]
29. Oliveira, L.; Silva, M.C.; Gomes, A.P.; Santos, R.F.; Cardoso, M.S.; Nóvoa, A.; Luche, H.; Cavadas, B.; Amorim, I.; Gärtner, F.; et al. CD5L as a promising biological therapeutic for treating sepsis. *Nat. Commun.* **2024**, *15*, 4119. [CrossRef]
30. Sanjurjo, L.; Aran, G.; Téllez, É.; Amézaga, N.; Armengol, C.; López, D.; Prats, C.; Sarrias, M.-R. CD5L Promotes M2 Macrophage Polarization through Autophagy-Mediated Upregulation of ID3. *Front. Immunol.* **2018**, *9*, 480. [CrossRef]
31. Cambier, S.; Gouwy, M.; Proost, P. The chemokines CXCL8 and CXCL12: Molecular and functional properties, role in disease and efforts towards pharmacological intervention. *Cell. Mol. Immunol.* **2023**, *20*, 217–251. [CrossRef]
32. Wu, J.; Liu, X.; Wu, J.; Lou, C.; Zhang, Q.; Chen, H.; Yang, Z.; Long, S.; Wang, Y.; Shang, Z.; et al. CXCL12 derived from CD248-expressing cancer-associated fibroblasts mediates M2-polarized macrophages to promote nonsmall cell lung cancer progression. *Biochim. Biophys. Acta (BBA) Mol. Basis Dis.* **2022**, *1868*, 166521. [CrossRef] [PubMed]
33. Deng, W.; Yi, C.; Pan, W.; Liu, J.; Qi, J.; Chen, J.; Zhou, Z.; Duan, Y.; Ning, X.; Li, J.; et al. Vascular Cell Adhesion Molecule-1 (VCAM-1) contributes to macular fibrosis in neovascular age-related macular degeneration through modulating macrophage functions. *Immun. Ageing* **2023**, *20*, 65. [CrossRef]
34. Abdallah, F.; Coindre, S.; Gardet, M.; Meurisse, F.; Naji, A.; Suganuma, N.; Abi-Rached, L.; Lambotte, O.; Favier, B. Leukocyte Immunoglobulin-Like Receptors in Regulating the Immune Response in Infectious Diseases: A Window of Opportunity to Pathogen Persistence and a Sound Target in Therapeutics. *Front. Immunol.* **2021**, *12*, 717998. [CrossRef]
35. Dorighello, G.G.; Assis, L.H.P.; Rentz, T.; Morari, J.; Santana, M.F.M.; Passarelli, M.; Ridgway, N.D.; Vercesi, A.E.; Oliveira, H.C.F. Novel Role of CETP in Macrophages: Reduction of Mitochondrial Oxidants Production and Modulation of Cell Immune-Metabolic Profile. *Antioxidants* **2022**, *11*, 1734. [CrossRef]
36. Xue, J.D.; Gao, J.; Tang, A.F.; Feng, C. Shaping the immune landscape: Multidimensional environmental stimuli refine macrophage polarization and foster revolutionary approaches in tissue regeneration. *Heliyon* **2024**, *10*, e37192. [CrossRef]
37. Yaseen, H.; Butenko, S.; Polishuk-Zotkin, I.; Schif-Zuck, S.; Pérez-Sáez, J.M.; Rabinovich, G.A.; Ariel, A. Galectin-1 Facilitates Macrophage Reprogramming and Resolution of Inflammation Through IFN-β. *Front. Pharmacol.* **2020**, *11*, 901. [CrossRef]
38. Nakamura, K.; Smyth, M.J. TREM2 marks tumor-associated macrophages. *Signal Transduct. Target. Ther.* **2020**, *5*, 233. [CrossRef]
39. Revel, M.; Sautès-Fridman, C.; Fridman, W.H.; Roumenina, L.T. C1q+ macrophages: Passengers or drivers of cancer progression. *Trends Cancer* **2022**, *8*, 517–526. [CrossRef] [PubMed]
40. Zhang, S.; Peng, W.; Wang, H.; Xiang, X.; Ye, L.; Wei, X.; Wang, Z.; Xue, Q.; Chen, L.; Su, Y.; et al. C1q+ tumor-associated macro-phages contribute to immunosuppression through fatty acid metabolic reprogramming in malignant pleural effusion. *J. Immunother. Cancer* **2023**, *11*, e007441. [CrossRef] [PubMed] [PubMed Central]
41. Vidergar, R.; Biswas, S.K. Metabolic regulation of Cathepsin B in tumor macrophages drives their pro-metastatic function. *Cancer Cell* **2022**, *40*, 1079–1081. [CrossRef]
42. Wang, J.; Zheng, M.; Yang, X.; Zhou, X.; Zhang, S. The Role of Cathepsin B in Pathophysiologies of Non-tumor and Tumor tissues: A Systematic Review. *J. Cancer* **2023**, *14*, 2344–2358. [CrossRef]
43. Haidar, B.; Kiss, R.S.; Sarov-Blat, L.; Brunet, R.; Harder, C.; McPherson, R.; Marcel, Y.L. Cathepsin D, a lysosomal protease, regulates ABCA1-mediated lipid efflux. *J. Biol. Chem.* **2006**, *281*, 39971–39981. [CrossRef]
44. Lee, S.G.; Woo, S.M.; Seo, S.U.; Lee, C.-H.; Baek, M.-C.; Jang, S.H.; Park, Z.Y.; Yook, S.; Nam, J.-O.; Kwon, T.K. Cathepsin D promotes polarization of tumor-associated macrophages and metastasis through TGFBI-CCL20 signaling. *Exp. Mol. Med.* **2024**, *56*, 383–394. [CrossRef]
45. Zheng, P.; Luo, Q.; Wang, W.; Li, J.; Wang, T.; Wang, P.; Chen, L.; Zhang, P.; Chen, H.; Liu, Y.; et al. Tumor-associated macrophages-derived exosomes promote the migration of gastric cancer cells by transfer of functional Apolipoprotein E. *Cell Death Dis.* **2018**, *9*, 434. [CrossRef]
46. Huo, R.; Zhao, R.; Li, Z.; Li, M.; Bin, Y.; Wang, D.; Xue, G.; Wu, J.; Lin, X. APOE expression in papillary thyroid carcinoma: Influencing tumor progression and macrophage polarization. *Immunobiology* **2024**, *229*, 152821. [CrossRef]
47. Ren, L.; Yi, J.; Yang, Y.; Li, W.; Zheng, X.; Liu, J.; Li, S.; Yang, H.; Zhang, Y.; Ge, B.; et al. Systematic pan-cancer analysis identifies APOC1 as an immunological biomarker which regulates macrophage polarization and promotes tumor metastasis. *Pharmacol. Res.* **2022**, *183*, 106376. [CrossRef] [PubMed]
48. Zhang, J.; Li, S.; Liu, F.; Yang, K. Role of CD68 in tumor immunity and prognosis prediction in pan-cancer. *Sci. Rep.* **2022**, *12*, 7844. [CrossRef] [PubMed]

49. Li, H.; Miao, Y.; Zhong, L.; Feng, S.; Xu, Y.; Tang, L.; Wu, C.; Zhang, X.; Gu, L.; Diao, H.; et al. Identification of TREM2-positive tumor-associated macrophages in esophageal squamous cell carcinoma: Implication for poor prognosis and immunotherapy modulation. *Front. Immunol.* **2023**, *14*, 1162032. [CrossRef] [PubMed]
50. Lyu, L.; Yao, J.; Wang, M.; Zheng, Y.; Xu, P.; Wang, S.; Zhang, D.; Deng, Y.; Wu, Y.; Yang, S.; et al. Overexpressed Pseudogene. *Front. Oncol.* **2020**, *10*, 1245. [CrossRef]
51. Wang, W.-C.; Lin, Y.-S.; Chang, Y.-F.; Yeh, C.-C.; Su, C.-T.; Wu, J.-S.; Su, F.-H. Association of HLA-DPA1, HLA-DPB1, and HLA-DQB1 Alleles with the Long-Term and Booster Immune Responses of Young Adults Vaccinated Against the Hepatitis B Virus as Neonates. *Front. Immunol.* **2021**, *12*, 710414. [CrossRef]
52. Mao, X.; Xu, J.; Wang, W.; Liang, C.; Hua, J.; Liu, J.; Zhang, B.; Meng, Q.; Yu, X.; Shi, S. Crosstalk between cancer-associated fibroblasts and immune cells in the tumor microenvironment: New findings and future perspectives. *Mol. Cancer* **2021**, *20*, 131. [CrossRef]
53. Chu, X.; Tian, Y.; Lv, C. Decoding the spatiotemporal heterogeneity of tumor-associated macrophages. *Mol. Cancer* **2024**, *23*, 150. [CrossRef] [PubMed]
54. Piollet, M.; Porsch, F.; Rizzo, G.; Kapser, F.; Schulz, D.J.J.; Kiss, M.G.; Schlepckow, K.; Morenas-Rodriguez, E.; Sen, M.O.; Gropper, J.; et al. TREM2 protects from atherosclerosis by limiting necrotic core formation. *Nat. Cardiovasc. Res.* **2024**, *3*, 269–282. [CrossRef] [PubMed]
55. Zhou, L.; Wang, M.; Guo, H.; Hou, J.; Zhang, Y.; Li, M.; Wu, X.; Chen, X.; Wang, L. Integrated Analysis Highlights the Immunosuppressive Role of TREM2. *Front. Immunol.* **2022**, *13*, 848367.
56. Adawy, A.; Komohara, Y.; Hibi, T. Tumor-associated macrophages: The key player in hepatoblastoma microenvironment and the promising therapeutic target. *Microbiol. Immunol.* **2024**, *68*, 249–253. [CrossRef]
57. Larionova, I.; Kazakova, E.; Patysheva, M.; Kzhyshkowska, J. Transcriptional, Epigenetic and Metabolic Programming of Tumor-Associated Macrophages. *Cancers* **2020**, *12*, 1411. [CrossRef]
58. Khantakova, D.; Brioschi, S.; Molgora, M. Exploring the Impact of TREM2 in Tumor-Associated Macrophages. *Vaccines* **2022**, *10*, 943. [CrossRef]
59. Hu, W.-M.; Yang, Y.-Z.; Zhang, T.-Z.; Qin, C.-F.; Li, X.-N. LGALS3 Is a Poor Prognostic Factor in Diffusely Infiltrating Gliomas and Is Closely Correlated with CD163+ Tumor-Associated Macrophages. *Front. Med.* **2020**, *7*, 182. [CrossRef]
60. Peshoff, M.M.; Gupta, P.; Oberai, S.; Trivedi, R.; Katayama, H.; Chakrapani, P.; Dang, M.; Migliozzi, S.; Gumin, J.; Kadri, D.B.; et al. Triggering receptor expressed on myeloid cells 2 (TREM2) regulates phagocytosis in glioblastoma. *Neuro-Oncology* **2024**, *26*, 826–839. [CrossRef]
61. Cignarella, F.; Filipello, F.; Bollman, B.; Cantoni, C.; Locca, A.; Mikesell, R.; Manis, M.; Ibrahim, A.; Deng, L.; Benitez, B.A.; et al. TREM2 activation on microglia promotes myelin debris clearance and remyelination in a model of multiple sclerosis. *Acta Neuropathol.* **2020**, *140*, 513–534. [CrossRef]
62. Chen, J.; Zhu, T.; Jiang, G.; Zeng, Q.; Li, Z.; Huang, X. Target delivery of a PD-1-TREM2 scFv by CAR-T cells enhances anti-tumor efficacy in colorectal cancer. *Mol. Cancer* **2023**, *22*, 131. [CrossRef]
63. Wang, Q.; Wu, Y.; Jiang, G.; Huang, X. Galectin-3 induces pathogenic immunosuppressive macrophages through interaction with TREM2 in lung cancer. *J. Exp. Clin. Cancer Res.* **2024**, *43*, 224. [CrossRef]
64. Brosseau, C.; Colas, L.; Magnan, A.; Brouard, S. CD9 Tetraspanin: A New Pathway for the Regulation of Inflammation? *Front. Immunol.* **2018**, *9*, 2316. [CrossRef]
65. Hwang, J.W.; Cho, Y.; Bae, G.U.; Kim, S.N.; Kim, Y.K. Protein arginine methyltransferases: Promising targets for cancer therapy. *Exp. Mol. Med.* **2021**, *53*, 788–808. [CrossRef]
66. Ma, R.Y.; Black, A.; Qian, B.Z. Macrophage diversity in cancer revisited in the era of single-cell omics. *Trends Immunol.* **2022**, *43*, 546–563. [CrossRef]